

The infrared bands of polycyclic aromatic hydrocarbons in the 1.6–1.7 μm wavelength region

Tao Chen^{1,*}, Yi Luo^{1,2,**}, and Aigen Li^{2,***}

¹ School of Engineering Sciences in Chemistry, Biotechnology and Health, Department of Theoretical Chemistry and Biology, Royal Institute of Technology, 10691, Stockholm, Sweden

² Hefei National Laboratory for Physical Science at the Microscale, Department of Chemical Physics, School of Chemistry and Materials Science, University of Science and Technology of China, Hefei, 230026 Anhui, China

³ Department of Physics and Astronomy, University of Missouri, Columbia, MO 65211, USA

November 24, 2021

ABSTRACT

Context. The 3.3 μm aromatic C–H stretching band of polycyclic aromatic hydrocarbon (PAH) molecules seen in a wide variety of astrophysical regions is often accompanied by a series of weak satellite bands at ~ 3.4 – $3.6 \mu\text{m}$. One of these sources, IRAS 21282+5050, a planetary nebula, also exhibits a weak band at $\sim 1.68 \mu\text{m}$. While the satellite features at ~ 3.4 – $3.6 \mu\text{m}$ are often attributed to the anharmonicities of PAHs, it is not clear whether overtones or combination bands dominate the 1.68 μm feature.

Aims. In this work, we examine the anharmonic spectra of eight PAH molecules, including anthracene, tetracene, pentacene, phenanthrene, chrysene, benz[a]anthracene, pyrene, and perylene, to explore the origin of the infrared bands in the 1.6–1.7 μm wavelength region.

Methods. Density Functional Theory (DFT) in combination with the vibrational second-order perturbation theory (VPT2) is utilized for computing the anharmonic spectra of PAHs. To simulate the vibrational excitation process of PAHs, the Wang-Landau random walk technique is employed.

Results. All the dominant bands in the 1.6–1.7 μm wavelength range and in the 3.1–3.5 μm C–H stretching region are calculated and tabulated. It is demonstrated that combination bands dominate the 1.6–1.7 μm region, while overtones are rare and weak in this region. We also calculate the intensity ratios of the 3.1–3.5 μm C–H stretching features to the bands in the 1.6–1.7 μm region, $I_{3.1-3.5}/I_{1.6-1.7}$, for both ground and vibrationally excited states. On average, we obtain $\langle I_{3.1-3.5}/I_{1.6-1.7} \rangle \approx 12.6$ and $\langle I_{3.1-3.5}/I_{1.6-1.7} \rangle \approx 17.6$ for PAHs at ground states and at vibrationally excited states, respectively.

Key words. astrochemistry, molecular data, molecular processes, ISM: lines and bands, infrared: general, ISM: molecules

1. Introduction

The broad infrared (IR) emission bands at 3.3, 6.2, 7.7, 8.6, and 11.3 μm observed in a wide variety of Galactic and extragalactic objects are generally attributed to polycyclic aromatic hydrocarbon (PAH) molecules (Leger & Puget 1984; Allamandola et al. 1989). These bands account for ~ 10 – 20% of the total IR emission of the Milky Way and star-forming galaxies (Tielens 2008). Besides these five prominent bands, a few minor bands are also widely observed, e.g., the band at $\sim 3.4 \mu\text{m}$ which is often attributed to the C–H stretch of aliphatic hydrocarbons (Pendleton & Allamandola 2002), superhydrogenated PAHs (Bernstein et al. 1996; Sandford & Bernstein 2013), or anharmonicity (Barker et al. 1987), and in some objects, multiple weaker features at 3.46, 3.51, and 3.56 μm are also observed, with a tendency to decrease in strength with increasing wavelength (Geballe et al. 1985; Jourdain de Muizon et al. 1986; Joblin et al. 1996). In addition, a weak band at $\sim 1.68 \mu\text{m}$

is seen in IRAS 21282+5050, a planetary nebula (Geballe et al. 1994).¹

There is a debate on the origin of the bands in the 1.6–1.7 μm wavelength region. Brenner & Barker (1992) predicted the intensity ratio of the 1.68 μm band to the 3.4 μm band to be $I_{1.68}/I_{3.4} \approx 1/6$, provided that the 3.4 μm feature arises from the $\nu = 2 \rightarrow 1$ transition while the 1.68 μm feature arises from the $\nu = 2 \rightarrow 0$ overtone emission, where ν is the vibrational quantum number. However, observationally, Siebenmorgen & Peletier (1993) derived $I_{1.68}/I_{3.4} \lesssim 1/48$ and Magazzù & Strazzulla (1992) derived $I_{1.68}/I_{3.4} \lesssim 1/45$. Duley (1994) argued that the 1.68 μm feature could not be attributed to the overtones of the C–H stretch, instead, it could result from combination bands. On the other hand, experimentally, Reddy et al. (1982) detected a band at $\sim 1.67 \mu\text{m}$ in the spectra of highly vibrationally excited benzene and attributed it to the overtone transition.

¹ Attempts to search for the 1.68 μm feature in the planetary nebula Hb 5 (Magazzù & Strazzulla 1992), the protoplanetary nebula HD 44179, the planetary nebula He 2–177, and the photodissociated region Orion bar (Siebenmorgen & Peletier 1993) have been made but only upper limits have been placed.

* Email: taochen@kth.se

** Email: luo@kth.se

*** Email: lia@missouri.edu

The theoretical anharmonic spectra of PAHs contain detailed information about each vibrational mode (Mackie et al. 2015, 2016, 2018a), which ought to provide conclusive evidence regarding the essence of the bands in the 1.6–1.7 μm wavelength region. Anharmonic spectra can be calculated with *ab initio* methods, which, in theory, has been well established for decades (Clabo et al. 1988; Allen et al. 1990; Amos et al. 1991; Maslen et al. 1992; Martin et al. 1995; Assfeld et al. 1995). However, due to high computational costs, in practice, the calculation of anharmonic spectra for large molecules, e.g., PAHs, emerges only recently.

Maltseva et al. (2015, 2016, 2018) measured the IR absorption spectra at very low temperature ($\sim 4\text{K}$) by means of the UV-IR ion dip spectroscopy, allowing them to obtain high-resolution IR spectra of PAHs. Nevertheless, such spectra can hardly be interpreted by harmonic models. To interpret the measured spectra, Mackie et al. (2015, 2016, 2018a) calculated the ground-state anharmonic IR spectra for linear, non-linear, hydrogenated and methylated PAHs using the second-order vibrational perturbations theory (VPT2). Although for most of the bands their calculated spectra accurately match the high-resolution experimental spectra, Maltseva et al. (2015) noticed that there are several intensive bands still missing in the C–H stretch region of the calculated spectra. Chen (2018) accounted for the missing bands through the inclusion of the 1-3 and 2-2 Darling-Dennison resonances in the VPT2 calculations. To model the astronomical environments and interpret the observations, Mackie et al. (2018b) and Chen et al. (2018) incorporated vibrational excitations in the calculations of the anharmonic spectra using the Wang-Landau random walk technique. This approach generated reasonable emission spectra in comparison with the experimental spectra measured by the Berkeley Single Photon InfraRed Emission Spectrometer (Schlemmer et al. 1994; Wagner et al. 2000).

In this work, we compute the ground-state and vibrationally-excited anharmonic spectra of a number of PAH species to explore the origin of the bands in the 1.6–1.7 μm wavelength region and compare the strengths of the bands in this region with that of the C–H stretch in the 3.1–3.5 μm region.

2. Computational details

The anharmonic vibrational spectra are calculated using the density of functional theory (DFT) as implemented in the Gaussian 16 package (Frisch et al. 2016). The functional of B3LYP (Becke 1992; Lee et al. 1988) in combination with the polarized double- ζ basis set, N07D (Barone et al. 2014), are utilized for the calculations. It has been shown that such a combination produces more accurate spectra in comparison with other DFT methods (Mackie et al. 2018a; Chen 2018).

The geometry optimizations are performed with a very tight convergence criterion and a very fine integration grid (Int = 200 974) for numerical integrations. For the resonant calculation, the generalized VPT2 (GVPT2) approach (Barone et al. 2014) is used. GVPT2 involves a two-step procedure: first, resonant terms are identified by means of an ad hoc test (Martin et al. 1995) and successively removed, which is called deperturbed VPT2 (DVPT2). In the second step, the discarded terms are reintroduced through a variational treatment. This approach has been recognized

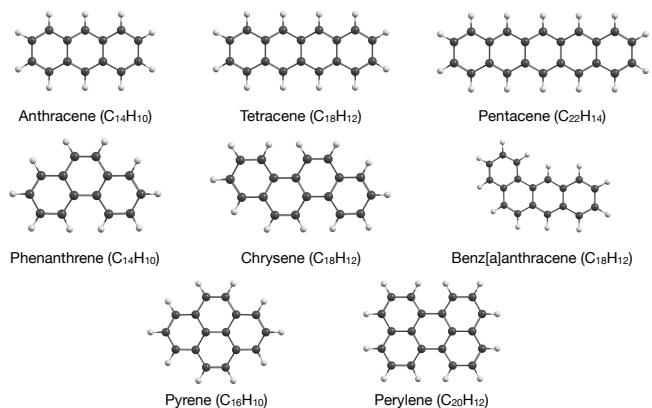


Fig. 1. The Molecules studied in this work. Anthracene, tetracene and pentacene are linear PAHs. Phenanthrene, chrysene and benz[a]anthracene are non-linear PAHs. Pyrene and perylene are compact PAHs.

to give accurate results (Maslen et al. 1992; Boese & Martin 2004; Barone et al. 2014; Mackie et al. 2015, 2016; Martin et al. 1995).

To balance the computational costs and accuracy of anharmonic IR spectra, only 1-2 Fermi resonances, 1-1 and 2-2 Darling-Dennison resonances are taken into account. The maximum resonant thresholds are set to 200 cm^{-1} for both types of resonances, and the minimum thresholds are all set to 0 cm^{-1} . Such settings have been evaluated and produced reasonable spectra (Chen 2018).

3. Results and discussion

The molecules studied in this work are shown in Figure 1. They can roughly be divided to three groups: (i) linear PAHs including anthracene ($\text{C}_{14}\text{H}_{10}$), tetracene ($\text{C}_{18}\text{H}_{12}$) and pentacene ($\text{C}_{22}\text{H}_{14}$); (ii) non-linear PAHs including phenanthrene ($\text{C}_{14}\text{H}_{10}$), chrysene ($\text{C}_{18}\text{H}_{12}$) and benz[a]anthracene ($\text{C}_{18}\text{H}_{12}$); and (iii) compact or pericondensed PAHs including pyrene ($\text{C}_{16}\text{H}_{10}$) and perylene ($\text{C}_{20}\text{H}_{12}$). The symmetries of these molecules are as follows: naphthalene (D_{2h}), anthracene (D_{2h}), tetracene (D_{2h}), phenanthrene (C_{2v}), chrysene (C_{2h}), benz[a]anthracene (C_s), pyrene (D_{2h}) and perylene (D_{2h}).

3.1. The importance of anharmonicity

For harmonic oscillators, the vibrational states are equally separated on symmetric closed parabolic potential energy surface. The vibrational energies at each state can be calculated from the following equation:

$$E_{\text{harm}}(n) = \sum_i h\nu_i \left(n_i + \frac{1}{2} \right), \quad (1)$$

where ν_i is the frequency of the i -th vibrational mode. $n \equiv (n_1, n_2, \dots)$ represents the quantum number of each vibrational state. The fundamental vibrational energy corresponds to the transition from the ground ($n = 0$) to the first vibrational state ($n = 1$), i.e., $E(1) = (3/2) \sum_i h\nu_i$. The calculated fundamental bands for the studied molecules in the 1.5–3.5 μm wavelength region are shown in Figure 2. The insets in Figure 2 expand the 1.6–1.7 μm region. It is clear that the fundamental bands for PAHs are only present

in the C–H stretch region at $\sim 3.1\text{--}3.5 \mu\text{m}$ and no bands are seen in the 1.6–1.7 μm region.

According to Eq. 1, a molecule bonded by harmonic potential might reach infinite energy $E(n \rightarrow \infty)$ without bond breaking. However, this is not the case in reality. Molecules do dissociate at highly excited vibrationally states (Chen et al. 2015; Chen & Luo 2019). The potential energy surface is not a symmetric parabolic shape, in contrast, it is a non-symmetric open well (anharmonic potential), which allows a molecule to break at certain vibrationally state. On an anharmonic potential energy surface, the energy levels are unequally separated, which can be computed as follows:

$$E_{\text{anharm}}(n) = \sum_i h\nu_i \left(n_i + \frac{1}{2} \right) + \sum_{i \leq j} \chi_{ij} \left(n_i + \frac{1}{2} \right) \left(n_j + \frac{1}{2} \right) \quad (2)$$

where χ_{ij} represents the anharmonic coupling which describes the interactions (mode couplings) or resonances among various vibrational modes and is usually given by a 2-dimensional matrix. Since most of the elements of χ_{ij} are negative, the anharmonic energy levels $E_{\text{anharm}}(n)$ are lower than the corresponding harmonic energy levels $E_{\text{harm}}(n)$. Therefore, with anharmonic potential, the positions and intensities of the fundamental bands differ from that of harmonic potential. Moreover, due to mode couplings, combination bands (i.e., two or more fundamental vibrations are excited simultaneously) show up in the spectra (Mackie et al. 2015; Maltseva et al. 2015).

Figure 3 shows the anharmonic spectra of the studied PAHs. Due to anharmonic effects, more bands (e.g., combination bands) appear in the C–H stretch region and the fundamental bands systemically shift to longer wavelengths in comparison with Figure 2. The insets in Figure 3 amplify the 1.6–1.7 μm region. Unlike Figure 2, multiple weak bands show up in this region. The mode numbers, wavelengths and absolute intensities for the C–H stretch and 1.6–1.7 μm regions are given in the Appendix, in addition, the mode descriptions (including frequencies, symmetries, and displacement vectors) for the modes contributing to these two regions can also be found in the Appendix. One can see that the 1.6–1.7 μm region is dominated by the combination bands and no intensive overtone can be found in this region for linear (e.g., anthracene, tetracene and pentacene) and compact (e.g., pyrene and perylene) PAHs, since the first overtones (for the fundamental bands in the C–H stretch region) are electric-dipole-forbidden (Duley 1994).

Only a few overtones can be seen for non-linear PAHs (e.g., phenanthrene, benz[a]anthracene). The highest intensity of the overtones among all the studied molecules is $\sim 2.683 \text{ km mol}^{-1}$ which comes from the 1.66 μm band of benz[a]anthracene, and it corresponds to the overtone of the fundamental band ν_{10} . The second highest overtone comes from phenanthrene with an intensity of $\sim 1.434 \text{ km mol}^{-1}$, which corresponds to the overtone of the fundamental band ν_9 .

3.2. Vibrational excitations

Molecules in the ISM are mostly excited by starlight (i.e., UV and visible photons). Following the internal conversion, the absorbed energies are rapidly transferred to nuclear de-

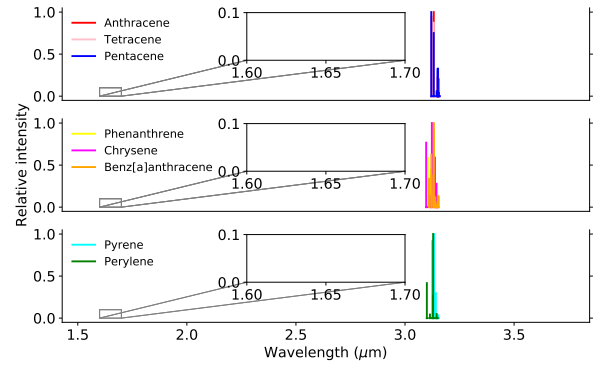


Fig. 2. Calculated harmonic fundamental bands of anthracene, tetracene, pentacene, phenanthrene, chrysene, benz[a]anthracene, pyrene and perylene. The insets zoom in the 1.6–1.7 μm region.

grees of freedom, i.e., vibrational excited states. At a vibrationally excited state, the IR spectrum differs significantly from that of the ground state (Chen et al. 2018; Mackie et al. 2018b). Moreover, PAHs may dissociate to smaller fragments or isomerize to multiple structures at a high vibrational state, in which anharmonicity plays a key role (Chen & Luo 2019). To incorporate the vibrational excitations, the vibrational microcanonical density of states (DoS) is calculated following the Wang–Landau random walk model (Wang & Landau 2001). In the model, the initial density of states $g(E)$ is set to 1 for all possible energies E . Then, a random walk in energy space is begun by forming trial states, each of which is produced by randomly picking a quanta n_i and randomly changing its value ($+1$, 0 , or -1). In general, if E_1 and E_2 are energies before and after a quanta set is changed, the transition probability from energy E_1 to E_2 is

$$p(E_1 \rightarrow E_2) = \min \left\{ \frac{g(E_1)}{g(E_2)}, 1 \right\}, \quad (3)$$

which implies that if $g(E_2) \leq g(E_1)$, the state with energy E_2 is accepted, otherwise it is accepted with a probability $g(E_1)/g(E_2)$. In addition, the maximum vibrational states have to be considered. All the vibrational quantum number is chosen such that the associated energy remains in the increasing region.

The vibrational DoS provides the weights needed to achieve flat-histogram sampling in energy space (Basire et al. 2009). Following the trend of the DoS, second random walks in the space of quantum numbers are performed to build the accumulated absorption $I(\nu, E)$ at the wavelength ν and for a given internal energy. The absorption intensity $I(\nu, T)$ at finite temperature T can be derived by a standard Laplace transformation of the accumulated absorption $I(\nu, E)$:

$$I(\nu, T) = \frac{1}{Z} \int I(\nu, E) \Omega(E) \exp(-E/k_B T) dE, \quad (4)$$

where $\Omega(E)$ represents the DoS, k_B is the Boltzmann constant, and Z is the partition function:

$$Z = \int \Omega(E) \exp(-E/k_B T) dE, \quad (5)$$

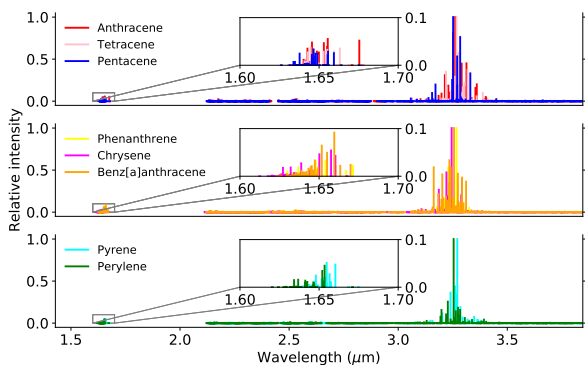


Fig. 3. Calculated anharmonic IR spectra (including fundamental bands, combination bands and overtones) of anthracene, tetracene, pentacene, phenanthrene, chrysene, benz[a]anthracene, pyrene and perylene at ground states. The insets zoom in the 1.6–1.7 μm region.

Figure 4 shows the anharmonic IR spectra of eight molecules at 1000 K. At such high temperature, the bands are combined to several broad bands.

3.3. The band-intensity ratios of $I_{3.1-3.5}/I_{1.6-1.7}$

As shown in the Appendix, there are a large number of combination bands located in the 1.6–1.7 μm region. However, their average intensities are much lower than the bands in the C–H stretching region. To quantitate the differences between these two regions, we compute, $I_{3.1-3.5}/I_{1.6-1.7}$, the intensity ratios of the C–H stretch region and 1.6–1.7 μm region. In the calculations, the C–H stretch region is measured from 2800–3200 cm^{-1} , i.e., 3.125–3.571 μm , while the 1.6–1.7 μm region is measured from 5900–6300 cm^{-1} , i.e., 1.587–1.695 μm .

Table 1 shows the ratios calculated from the intensities in both regions. At ground vibrational states, pentacene shows the highest ratio (~ 13.27). At excited vibrational states, the highest ratio comes from perylene. No general trend as a function of molecular size or structure is found; however, for linear molecules at ground state, the ratio appears to increase with the number of aromatic rings. The average ratio of the studied molecules at ground states are $\langle I_{3.1-3.5}/I_{1.6-1.7} \rangle \approx 12.6$. For vibrationally excited states, the average ratio is $\langle I_{3.1-3.5}/I_{1.6-1.7} \rangle \approx 17.6$. We notice that the ratios increase ~ 10 –50% going from ground states to excited states. Hence, for PAHs, the band ratio of 12.6 ought to be a lower limit.

4. Conclusions

Using DFT in combination with the VPT2 method, the 1.6–1.7 μm region of the IR spectra of PAHs is investigated. The calculations reveal that anharmonicity and mode couplings are crucial for this region, in which combination bands are more intensive and abundant than the overtones. Only two of the eight molecules considered here exhibit overtones in this region (i.e., phenanthrene and benz[a]anthracene, with a maximum intensity of $\sim 2.683 \text{ km mol}^{-1}$).

To model the vibrational excitations of these molecules, the Wang-Landau random walk algorithm is incorporated.

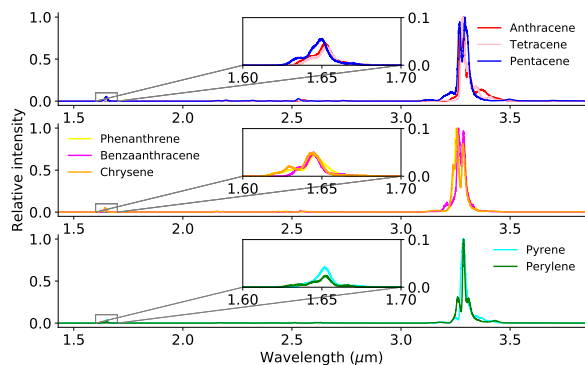


Fig. 4. Calculated anharmonic IR spectra of anthracene, tetracene, pentacene, phenanthrene, chrysene, benz[a]anthracene, pyrene and perylene at 1000 K.

The model shows that, due to anharmonicity and vibrational excitations, the fundamental and combination bands (at the ground state) are merged to several inseparable broad bands. The C–H stretching region at 3.1–3.5 μm is compared to the 1.6–1.7 μm region. The average band intensity ratios are $\langle I_{3.1-3.5}/I_{1.6-1.7} \rangle \approx 12.6$ and $\langle I_{3.1-3.5}/I_{1.6-1.7} \rangle \approx 17.6$, respectively at ground states and at vibrationally excited states. Since the band intensity ratio $I_{3.1-3.5}/I_{1.6-1.7}$ goes up as the molecule gets excited, $\langle I_{3.1-3.5}/I_{1.6-1.7} \rangle \approx 12.6$ should be the lower-limit for PAHs.

Acknowledgements

We thank the anonymous referee for his/her very helpful comments which considerably improved the presentation of this work. This work is supported by the Swedish Research Council (Contract No. 2015–06501). The calculations were performed on resources provided by the Swedish National Infrastructure for Computing (SNIC). A.L. is supported in part by NSF AST-1816411 and NASA 80NSSC19K0572.

References

- Allamandola, L., Tielens, A., & Barker, J. 1989, The Astrophysical Journal Supplement Series, 71, 733
- Allen, W. D., Yamaguchi, Y., Császár, A. G., et al. 1990, Chemical Physics, 145, 427
- Amos, R. D., Handy, N. C., Green, W. H., et al. 1991, The Journal of Chemical Physics, 95, 8323
- Assfeld, X., Almlöf, J. E., & Truhlar, D. G. 1995, Chemical Physics Letters, 241, 438
- Barker, J. R., Allamandola, L., & Tielens, A. 1987, The Astrophysical Journal, 315, L61
- Barone, V., Biczysko, M., & Bloino, J. 2014, Physical Chemistry Chemical Physics, 16, 1759
- Basire, M., Parneix, P., Calvo, F., Pino, T., & Bréchnignac, P. 2009, The Journal of Physical Chemistry A, 113, 6947
- Becke, A. D. 1992, The Journal of Chemical Physics, 96, 2155
- Bernstein, M. P., Sandford, S. A., & Allamandola, L. J. 1996, The Astrophysical Journal Letters, 472, L127
- Boese, A. D. & Martin, J. M. 2004, The Journal of Physical Chemistry A, 108, 3085
- Brenner, J. & Barker, J. R. 1992, The Astrophysical Journal, 388, L39
- Chen, T. 2018, The Astrophysical Journal Supplement Series, 238, 18
- Chen, T., Gatchell, M., Stockett, M. H., et al. 2015, The Journal of Chemical Physics, 142, 144305
- Chen, T. & Luo, Y. 2019, Monthly Notices of the Royal Astronomical Society, 486, 1875

Table 1. The intensity ratio, $I_{3.1-3.5}/I_{1.6-1.7}$, of the C–H stretch to the bands in the 1.6–1.7 μm region (with 0 K for ground states and 1000 K for vibrational excited states. The “Max” column shows the ratios calculated based on the maximum intensities in each region. The “Sum” column is calculated based on the total intensities in each region.

Molecules	Max (0 K)	Sum (0 K)	Max (1000 K)	Sum (1000 K)
Anthracene	18.14	13.08	22.55	18.04
Tetracene	27.26	12.74	24.63	18.35
Pentacene	30.02	13.27	17.93	16.16
Phenanthrene	31.03	13.26	21.95	15.44
Chrysene	18.53	10.84	19.81	18.96
Benz[a]anthracene	10.91	12.96	20.05	13.99
Pyrene	19.65	12.98	23.78	17.72
Perylene	22.14	12.27	41.30	21.81
Mean	22.19	12.56	24.0	17.56

- Chen, T., Mackie, C., Candian, A., Lee, T. J., & Tielens, A. G. G. M. 2018, *Astronomy & Astrophysics*, 618, A49
- Clabo, D. A., Allen, W. D., Remington, R. B., Yamaguchi, Y., & Schaefer, H. F. 1988, *Chemical Physics*, 123, 187
- Duley, W. 1994, *The Astrophysical Journal*, 429, L91
- Frisch, M., Trucks, G., Schlegel, H., Scuseria, G., & et al. 2016, Wallingford CT
- Geballe, T., Joblin, C., d’Hendecourt, L., et al. 1994, *The Astrophysical Journal*, 434, L15
- Geballe, T., Lacy, J., Persson, S., McGregor, P., & Soifer, B. 1985, *The Astrophysical Journal*, 292, 500
- Joblin, C., Tielens, A., Allamandola, L., & Geballe, T. 1996, *The Astrophysical Journal*, 458, 610
- Jourdain de Muizon, M., Geballe, T., d’Hendecourt, L., Baas, F., et al. 1986, *Astrophysical Journal*, 306, L105
- Lee, C., Yang, W., & Parr, R. G. 1988, *Physical Review B*, 37, 785
- Leger, A. & Puget, J. 1984, *Astronomy and Astrophysics*, 137, L5
- Mackie, C. J., Candian, A., Huang, X., et al. 2015, *The Journal of Chemical Physics*, 143, 224314
- Mackie, C. J., Candian, A., Huang, X., et al. 2018a, *Phys. Chem. Chem. Phys.*, 20, 1189
- Mackie, C. J., Candian, A., Huang, X., et al. 2016, *The Journal of Chemical Physics*, 145, 084313
- Mackie, C. J., Chen, T., Candian, A., Lee, T. J., & Tielens, A. G. G. M. 2018b, *The Journal of Chemical Physics*, 149, 134302
- Magazzù, A. & Strazzulla, G. 1992, *Astronomy and Astrophysics*, 263, 281
- Maltseva, E., Mackie, C. J., Candian, A., et al. 2018, *Astronomy & Astrophysics*, 610, A65
- Maltseva, E., Petrignani, A., Candian, A., et al. 2015, *The Astrophysical Journal*, 814, 23
- Maltseva, E., Petrignani, A., Candian, A., et al. 2016, *The Astrophysical Journal*, 831, 58
- Martin, J. M., Lee, T. J., Taylor, P. R., & François, J.-P. 1995, *The Journal of Chemical Physics*, 103, 2589
- Maslen, P. E., Handy, N. C., Amos, R. D., & Jayatilaka, D. 1992, *The Journal of Chemical Physics*, 97, 4233
- Pendleton, Y. J. & Allamandola, L. J. 2002, *The Astrophysical Journal Supplement Series*, 138, 75
- Reddy, K., Heller, D. F., & Berry, M. J. 1982, *The Journal of Chemical Physics*, 76, 2814
- Sandford, S. A. & Bernstein, M. P. 2013, *The Astrophysical Journal Supplement Series*, 205, 8
- Schlemmer, S., Cook, D., Harrison, J., et al. 1994, *Science*, 265, 1686
- Siebenmorgen, R. & Peletier, R. 1993, *Astronomy and Astrophysics*, 279, L45
- Tielens, A. G. G. M. 2008, *Annu. Rev. Astron. Astrophys.*, 46, 289
- Wagner, D., Kim, H., & Saykally, R. 2000, *The Astrophysical Journal*, 545, 854
- Wang, F. & Landau, D. 2001, *Physical Review Letters*, 86, 2050

Appendix

Table 2. The dominant bands (with intensity $\gtrsim 0.2 \text{ km mol}^{-1}$) in C–H stretching region and $1.6\text{--}1.7 \mu\text{m}$ region for anthracene tetracene and pentacene. The symbol of "+" in the "Mode" column represents the combination bands between the modes on both sides of "+".

Anthracene			Tetracene			Pentacene		
Mode	Wavelength (μm)	Intensity (km mol^{-1})	Mode	Wavelength (μm)	Intensity (km mol^{-1})	Mode	Wavelength (μm)	Intensity (km mol^{-1})
ν_2	3.251	26.494	ν_1	3.269	0.263	ν_1	3.249	1.447
ν_3	3.261	32.837	ν_2	3.259	15.336	ν_2	3.252	67.771
ν_6	3.273	17.563	ν_3	3.267	52.686	ν_3	3.27	35.98
ν_7	3.306	3.858	ν_6	3.276	30.334	ν_5	3.275	0.207
ν_{10}	3.291	14.66	ν_7	3.318	19.531	ν_6	3.271	12.607
$\nu_{14}+\nu_{12}$	3.13	0.699	ν_{11}	3.293	5.278	ν_7	3.265	0.412
$\nu_{15}+\nu_{13}$	3.185	2.076	$\nu_{16}+\nu_{15}$	3.132	0.409	ν_{10}	3.331	22.409
$\nu_{15}+\nu_{14}$	3.214	10.125	$\nu_{17}+\nu_{14}$	3.146	0.483	ν_{11}	3.287	3.057
$\nu_{16}+\nu_{12}$	3.199	2.947	$\nu_{17}+\nu_{15}$	3.156	1.075	ν_{14}	3.284	51.692
$\nu_{16}+\nu_{15}$	3.305	5.656	$\nu_{18}+\nu_{13}$	3.137	0.702	$\nu_{21(2)}$	3.252	0.233
$\nu_{17}+\nu_{11}$	3.232	3.317	$\nu_{18}+\nu_{16}$	3.202	1.597	$\nu_{19}+\nu_{15}$	3.129	0.546
$\nu_{17}+\nu_{13}$	3.287	3.695	$\nu_{18}+\nu_{17}$	3.219	18.451	$\nu_{19}+\nu_{17}$	3.155	6.568
$\nu_{17}+\nu_{16}$	3.404	1.157	$\nu_{19}+\nu_{16}$	3.221	8.238	$\nu_{20}+\nu_{16}$	3.139	2.544
$\nu_{18}+\nu_{11}$	3.23	6.061	$\nu_{19}+\nu_{17}$	3.242	5.966	$\nu_{20}+\nu_{18}$	3.17	0.698
$\nu_{18}+\nu_{13}$	3.269	6.153	$\nu_{20}+\nu_{14}$	3.21	1.408	$\nu_{21}+\nu_{15}$	3.145	0.492
$\nu_{18}+\nu_{14}$	3.318	0.515	$\nu_{20}+\nu_{16}$	3.276	1.302	$\nu_{21}+\nu_{17}$	3.171	13.395
$\nu_{18}+\nu_{16}$	3.413	0.229	$\nu_{20}+\nu_{19}$	3.338	1.148	$\nu_{21}+\nu_{20}$	3.247	17.088
$\nu_{19}+\nu_{15}$	3.394	0.669	$\nu_{21}+\nu_{16}$	3.305	2.087	$\nu_{22}+\nu_{15}$	3.159	1.503
$\nu_{20}+\nu_{11}$	3.313	14.779	$\nu_{22}+\nu_{13}$	3.232	0.985	$\nu_{22}+\nu_{17}$	3.184	0.706
$\nu_{20}+\nu_{13}$	3.354	5.15	$\nu_{22}+\nu_{16}$	3.288	3.521	$\nu_{23}+\nu_{16}$	3.171	0.394
$\nu_{21}+\nu_{12}$	3.337	1.166	$\nu_{22}+\nu_{17}$	3.343	0.404	$\nu_{23}+\nu_{19}$	3.251	0.353
$\nu_{22}+\nu_{11}$	3.36	6.574	$\nu_{22}+\nu_{20}$	3.432	0.506	$\nu_{23}+\nu_{21}$	3.277	1.085
$\nu_{22}+\nu_{13}$	3.401	1.632	$\nu_{23}+\nu_{15}$	3.309	0.435	$\nu_{24}+\nu_{17}$	3.267	1.608
$\nu_{22}+\nu_{14}$	3.428	0.205	$\nu_{23}+\nu_{18}$	3.39	0.468	$\nu_{25}+\nu_{16}$	3.239	0.62
$\nu_2+\nu_1$	1.643	1.145	$\nu_{24}+\nu_{13}$	3.296	8.642	$\nu_{25}+\nu_{19}$	3.329	0.275
$\nu_3+\nu_1$	1.644	0.221	$\nu_{24}+\nu_{17}$	3.394	0.677	$\nu_{25}+\nu_{24}$	3.447	0.596
$\nu_4+\nu_2$	1.643	0.249	$\nu_{25}+\nu_{13}$	3.304	11.28	$\nu_{26}+\nu_{16}$	3.246	0.423
$\nu_4+\nu_3$	1.646	1.564	$\nu_{25}+\nu_{16}$	3.374	0.269	$\nu_{27}+\nu_{15}$	3.291	1.864
$\nu_5+\nu_2$	1.64	0.375	$\nu_{25}+\nu_{17}$	3.403	0.296	$\nu_{27}+\nu_{20}$	3.388	0.329
$\nu_6+\nu_1$	1.641	0.317	$\nu_{26}+\nu_{14}$	3.327	0.92	$\nu_{28}+\nu_{16}$	3.294	0.942
$\nu_6+\nu_4$	1.647	0.234	$\nu_{27}+\nu_{14}$	3.359	2.995	$\nu_{30}+\nu_{15}$	3.309	1.364
$\nu_6+\nu_5$	1.655	0.317	$\nu_{27}+\nu_{15}$	3.388	5.201	$\nu_{33}+\nu_{18}$	3.402	0.397
$\nu_7+\nu_4$	1.649	0.94	$\nu_2+\nu_1$	1.643	1.413	$\nu_{35}+\nu_{18}$	3.45	1.611
$\nu_7+\nu_5$	1.653	1.522	$\nu_3+\nu_1$	1.643	0.201	$\nu_{38}+\nu_{18}$	3.477	0.239
$\nu_8+\nu_3$	1.65	0.879	$\nu_4+\nu_2$	1.643	0.216	$\nu_2+\nu_1$	1.638	1.656
$\nu_8+\nu_6$	1.655	1.81	$\nu_4+\nu_3$	1.645	1.933	$\nu_4+\nu_3$	1.647	2.257
$\nu_8+\nu_7$	1.655	1.27	$\nu_5+\nu_2$	1.641	0.427	$\nu_5+\nu_2$	1.635	0.477
$\nu_{10}+\nu_9$	1.675	1.698	$\nu_6+\nu_1$	1.642	0.4	$\nu_6+\nu_1$	1.634	0.47
			$\nu_6+\nu_4$	1.647	0.238	$\nu_6+\nu_4$	1.643	0.241
			$\nu_6+\nu_5$	1.655	0.416	$\nu_6+\nu_5$	1.645	0.502
			$\nu_7+\nu_4$	1.648	1.001	$\nu_8+\nu_4$	1.646	1.047
			$\nu_7+\nu_5$	1.653	1.487	$\nu_8+\nu_5$	1.645	1.455
			$\nu_8+\nu_3$	1.649	1.056	$\nu_9+\nu_3$	1.648	1.182
			$\nu_8+\nu_6$	1.655	1.704	$\nu_9+\nu_6$	1.648	1.652
			$\nu_8+\nu_7$	1.654	1.491	$\nu_9+\nu_8$	1.649	1.623
			$\nu_{10}+\nu_9$	1.659	1.526	$\nu_{10}+\nu_7$	1.655	1.419
			$\nu_{12}+\nu_{11}$	1.663	1.85	$\nu_{10}+\nu_9$	1.647	0.324
						$\nu_{13}+\nu_{11}$	1.659	1.718
						$\nu_{14}+\nu_{12}$	1.656	1.93

Appendix

Table 3. Same as Table 2 but for phenanthrene, chrysene and benz[a]anthracene.

Phenanthrene			Chrysene			Benz[a]anthracene		
Mode	Wavelength (μm)	Intensity (km mol^{-1})	Mode	Wavelength (μm)	Intensity (km mol^{-1})	Mode	Wavelength (μm)	Intensity (km mol^{-1})
ν_1	3.23	14.189	ν_2	3.221	24.631	ν_1	3.241	15.535
ν_2	3.232	20.762	ν_6	3.245	52.127	ν_2	3.234	9.942
ν_3	3.253	4.707	ν_7	3.273	6.729	ν_3	3.263	1.973
ν_4	3.251	5.675	ν_{10}	3.292	20.111	ν_4	3.25	4.836
ν_5	3.267	44.507	ν_{11}	3.289	10.557	ν_5	3.256	29.281
ν_6	3.279	2.974	$\nu_{17}+\nu_{14}$	3.126	1.359	ν_6	3.293	12.017
ν_7	3.279	0.576	$\nu_{17}+\nu_{16}$	3.144	0.413	ν_7	3.282	0.934
ν_8	3.285	3.012	$\nu_{18}+\nu_{14}$	3.166	0.941	ν_8	3.275	1.614
ν_9	3.289	7.916	$\nu_{18}+\nu_{16}$	3.186	13.885	ν_9	3.274	13.356
ν_{10}	3.325	2.267	$\nu_{19}+\nu_{13}$	3.168	1.419	ν_{10}	3.284	3.289
$\nu_1(2)$	1.661	0.97	$\nu_{19}+\nu_{15}$	3.182	1.593	ν_{11}	3.299	3.102
$\nu_9(2)$	1.648	1.434	$\nu_{19}+\nu_{17}$	3.225	9.754	ν_{12}	3.311	10.633
$\nu_{10}(2)$	1.671	0.966	$\nu_{19}+\nu_{18}$	3.279	1.3	$\nu_4(2)$	1.652	1.881
$\nu_{14}(2)$	3.175	1.285	$\nu_{20}+\nu_{13}$	3.211	1.553	$\nu_5(2)$	1.67	0.698
$\nu_{15}(2)$	3.277	0.481	$\nu_{20}+\nu_{15}$	3.228	9.603	$\nu_8(2)$	1.642	0.264
$\nu_{14}+\nu_{12}$	3.13	0.724	$\nu_{20}+\nu_{18}$	3.319	0.644	$\nu_9(2)$	1.646	0.356
$\nu_{14}+\nu_{13}$	3.139	0.251	$\nu_{21}+\nu_{14}$	3.257	2.544	$\nu_{10}(2)$	1.66	2.683
$\nu_{15}+\nu_{13}$	3.178	2.586	$\nu_{21}+\nu_{16}$	3.268	1.028	$\nu_{12}(2)$	1.663	0.637
$\nu_{15}+\nu_{14}$	3.23	23.48	$\nu_{22}+\nu_{13}$	3.268	1.343	$\nu_{17}(2)$	3.195	1.603
$\nu_{16}+\nu_{11}$	3.189	0.39	$\nu_{22}+\nu_{15}$	3.289	0.882	$\nu_{18}(2)$	3.219	5.408
$\nu_{16}+\nu_{12}$	3.203	4.167	$\nu_{23}+\nu_{14}$	3.277	0.292	$\nu_{17}+\nu_{14}$	3.13	0.271
$\nu_{16}+\nu_{13}$	3.211	6.544	$\nu_{23}+\nu_{16}$	3.296	0.39	$\nu_{17}+\nu_{16}$	3.158	1.64
$\nu_{16}+\nu_{15}$	3.301	0.338	$\nu_{23}+\nu_{19}$	3.383	0.422	$\nu_{18}+\nu_{15}$	3.154	0.87
$\nu_{17}+\nu_{11}$	3.241	6.494	$\nu_{24}+\nu_{13}$	3.277	0.856	$\nu_{18}+\nu_{16}$	3.163	15.627
$\nu_{17}+\nu_{12}$	3.258	1.23	$\nu_{24}+\nu_{15}$	3.292	0.327	$\nu_{18}+\nu_{17}$	3.202	13.144
$\nu_{17}+\nu_{13}$	3.266	2.491	$\nu_{25}+\nu_{14}$	3.339	0.224	$\nu_{19}+\nu_{13}$	3.181	1.214
$\nu_{18}+\nu_{12}$	3.27	0.299	$\nu_{26}+\nu_{14}$	3.35	0.451	$\nu_{19}+\nu_{14}$	3.184	6.351
$\nu_{18}+\nu_{13}$	3.281	0.513	$\nu_{27}+\nu_{15}$	3.363	0.555	$\nu_{19}+\nu_{15}$	3.201	1.128
$\nu_{18}+\nu_{15}$	3.371	0.414	$\nu_{28}+\nu_{14}$	3.381	0.211	$\nu_{19}+\nu_{16}$	3.225	3.986
$\nu_{19}+\nu_{11}$	3.281	1.852	$\nu_2+\nu_1$	1.627	0.915	$\nu_{19}+\nu_{18}$	3.275	0.424
$\nu_{19}+\nu_{12}$	3.291	0.539	$\nu_4+\nu_3$	1.632	0.949	$\nu_{20}+\nu_{13}$	3.198	4.267
$\nu_{19}+\nu_{13}$	3.299	0.498	$\nu_6+\nu_5$	1.639	1.415	$\nu_{20}+\nu_{14}$	3.207	4.773
$\nu_{20}+\nu_{11}$	3.273	2.146	$\nu_7+\nu_5$	1.636	0.317	$\nu_{20}+\nu_{15}$	3.229	1.494
$\nu_{21}+\nu_{12}$	3.368	0.351	$\nu_8+\nu_6$	1.634	0.353	$\nu_{20}+\nu_{16}$	3.246	1.054
$\nu_{22}+\nu_{12}$	3.369	0.442	$\nu_8+\nu_7$	1.65	2.4	$\nu_{20}+\nu_{17}$	3.285	0.21
$\nu_3+\nu_2$	1.63	0.463	$\nu_9+\nu_7$	1.638	0.203	$\nu_{21}+\nu_{13}$	3.235	18.106
$\nu_4+\nu_3$	1.637	0.838	$\nu_{10}+\nu_8$	1.638	0.355	$\nu_{21}+\nu_{15}$	3.269	1.989
$\nu_6+\nu_3$	1.639	0.291	$\nu_{10}+\nu_9$	1.66	2.23	$\nu_{21}+\nu_{16}$	3.275	0.831
$\nu_6+\nu_4$	1.633	0.303	$\nu_{11}+\nu_5$	1.64	0.295	$\nu_{22}+\nu_{14}$	3.255	0.992
$\nu_7+\nu_4$	1.633	0.276	$\nu_{11}+\nu_8$	1.644	0.594	$\nu_{22}+\nu_{15}$	3.273	0.263
$\nu_7+\nu_6$	1.65	1.227	$\nu_{12}+\nu_6$	1.639	0.236	$\nu_{23}+\nu_{14}$	3.275	1.162
$\nu_8+\nu_6$	1.644	0.28	$\nu_{12}+\nu_7$	1.645	0.542	$\nu_{23}+\nu_{15}$	3.295	0.345
$\nu_8+\nu_7$	1.643	0.668	$\nu_{12}+\nu_{10}$	1.645	0.239	$\nu_{23}+\nu_{16}$	3.309	0.518
$\nu_9+\nu_4$	1.637	0.315	$\nu_{12}+\nu_{11}$	1.658	2.814	$\nu_{25}+\nu_{13}$	3.311	0.97
$\nu_9+\nu_6$	1.645	0.539				$\nu_{25}+\nu_{17}$	3.388	0.22
$\nu_9+\nu_8$	1.654	1.434				$\nu_{26}+\nu_{13}$	3.335	0.574
$\nu_{10}+\nu_5$	1.667	0.48				$\nu_{27}+\nu_{15}$	3.385	0.266
$\nu_{10}+\nu_9$	1.649	0.575				$\nu_6+\nu_5$	1.647	0.97
						$\nu_7+\nu_3$	1.64	0.238
						$\nu_7+\nu_4$	1.639	0.226
						$\nu_8+\nu_2$	1.639	0.335
						$\nu_9+\nu_6$	1.64	0.204
						$\nu_9+\nu_7$	1.645	0.617
						$\nu_{10}+\nu_5$	1.646	0.273
						$\nu_{10}+\nu_6$	1.645	0.568
						$\nu_{10}+\nu_8$	1.655	1.439
						$\nu_{11}+\nu_5$	1.649	0.493
						$\nu_{11}+\nu_9$	1.649	0.368
						$\nu_{11}+\nu_{10}$	1.643	0.457

Appendix

Table 4. Same as Table 2 but for pyrene and perylene.

Pyrene			Perylene		
Mode	Wavelength (μm)	Intensity (km mol^{-1})	Mode	Wavelength (μm)	Intensity (km mol^{-1})
ν_2	3.268	17.11	ν_2	3.227	19.342
ν_4	3.264	10.722	ν_3	3.24	3.259
ν_6	3.271	51.48	ν_6	3.284	11.855
ν_7	3.261	22.431	ν_7	3.254	75.684
ν_{10}	3.295	3.386	ν_{10}	3.259	4.774
$\nu_{14}+\nu_{13}$	3.129	0.366	$\nu_{16}+\nu_{15}$	3.131	2.005
$\nu_{15}+\nu_{12}$	3.148	1.3	$\nu_{18}+\nu_{14}$	3.141	0.472
$\nu_{15}+\nu_{13}$	3.157	1.312	$\nu_{19}+\nu_{15}$	3.194	5.775
$\nu_{16}+\nu_{12}$	3.202	6.022	$\nu_{19}+\nu_{17}$	3.198	11.821
$\nu_{16}+\nu_{13}$	3.219	2.167	$\nu_{20}+\nu_{13}$	3.194	0.703
$\nu_{17}+\nu_{11}$	3.2	2.747	$\nu_{20}+\nu_{16}$	3.22	7.837
$\nu_{17}+\nu_{14}$	3.24	18.711	$\nu_{20}+\nu_{18}$	3.253	1.574
$\nu_{17}+\nu_{15}$	3.285	9.817	$\nu_{20}+\nu_{19}$	3.305	4.553
$\nu_{17}+\nu_{16}$	3.362	1.78	$\nu_{21}+\nu_{13}$	3.221	1.25
$\nu_{18}+\nu_{14}$	3.28	2.257	$\nu_{21}+\nu_{16}$	3.258	1.841
$\nu_{18}+\nu_{15}$	3.311	0.424	$\nu_{21}+\nu_{18}$	3.3	0.607
$\nu_{18}+\nu_{16}$	3.381	1.424	$\nu_{21}+\nu_{19}$	3.338	2.793
$\nu_{19}+\nu_{11}$	3.255	9.365	$\nu_{22}+\nu_{14}$	3.274	13.828
$\nu_{19}+\nu_{14}$	3.318	1.12	$\nu_{22}+\nu_{15}$	3.264	10.669
$\nu_{19}+\nu_{15}$	3.347	0.626	$\nu_{22}+\nu_{17}$	3.28	6.801
$\nu_{20}+\nu_{11}$	3.253	0.609	$\nu_{22}+\nu_{20}$	3.384	0.975
$\nu_{20}+\nu_{14}$	3.308	0.595	$\nu_{22}+\nu_{21}$	3.415	0.277
$\nu_{20}+\nu_{15}$	3.348	3.847	$\nu_{23}+\nu_{13}$	3.246	1.278
$\nu_{21}+\nu_{12}$	3.331	0.792	$\nu_{23}+\nu_{16}$	3.321	0.467
$\nu_{21}+\nu_{13}$	3.327	1.585	$\nu_{23}+\nu_{19}$	3.367	0.616
$\nu_{22}+\nu_{12}$	3.318	2.181	$\nu_{24}+\nu_{13}$	3.259	0.575
$\nu_{23}+\nu_{13}$	3.365	1.941	$\nu_{24}+\nu_{14}$	3.271	1.358
$\nu_{24}+\nu_{11}$	3.375	0.965	$\nu_{24}+\nu_{17}$	3.297	1.098
$\nu_{24}+\nu_{14}$	3.428	0.241	$\nu_{24}+\nu_{20}$	3.403	1.177
$\nu_2+\nu_1$	1.648	1.254	$\nu_{25}+\nu_{13}$	3.325	1.371
$\nu_4+\nu_3$	1.652	0.81	$\nu_{25}+\nu_{18}$	3.393	3.126
$\nu_5+\nu_2$	1.641	0.211	$\nu_{26}+\nu_{15}$	3.368	0.525
$\nu_6+\nu_5$	1.657	1.409	$\nu_{27}+\nu_{16}$	3.383	1.225
$\nu_7+\nu_3$	1.644	0.24	$\nu_{30}+\nu_{13}$	3.382	1.195
$\nu_7+\nu_5$	1.653	0.952	$\nu_{31}+\nu_{17}$	3.463	0.485
$\nu_8+\nu_6$	1.654	1.062	$\nu_2+\nu_1$	1.634	1.127
$\nu_8+\nu_7$	1.655	2.62	$\nu_4+\nu_3$	1.637	1.191
$\nu_9+\nu_4$	1.657	0.555	$\nu_6+\nu_5$	1.643	0.836
$\nu_{10}+\nu_3$	1.655	0.44	$\nu_7+\nu_5$	1.641	0.723
$\nu_{10}+\nu_8$	1.648	0.642	$\nu_8+\nu_6$	1.642	0.78
$\nu_{10}+\nu_9$	1.66	2.441	$\nu_8+\nu_7$	1.641	1.042
			$\nu_9+\nu_6$	1.647	0.681
			$\nu_9+\nu_7$	1.646	0.256
			$\nu_{10}+\nu_8$	1.646	0.763
			$\nu_{10}+\nu_9$	1.652	2.587
			$\nu_{11}+\nu_5$	1.647	0.333
			$\nu_{11}+\nu_8$	1.646	0.252
			$\nu_{11}+\nu_9$	1.653	0.767
			$\nu_{12}+\nu_7$	1.646	0.349
			$\nu_{12}+\nu_{10}$	1.652	0.935
			$\nu_{12}+\nu_{11}$	1.653	3.418

Appendix

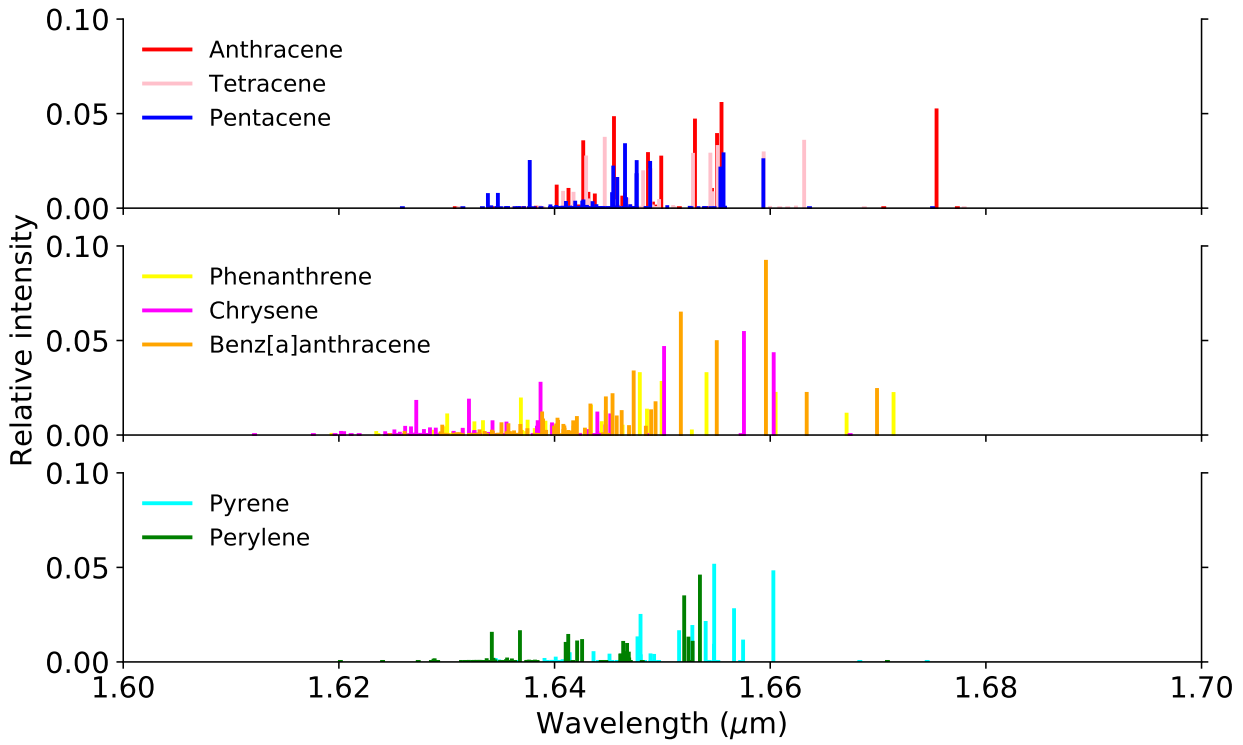


Fig. 5. The 1.6–1.7 μm region of the anharmonic IR spectra of ground-state anthracene, tetracene, pentacene, phenanthrene, chrysene benz[a]anthracene, pyrene and perylene.

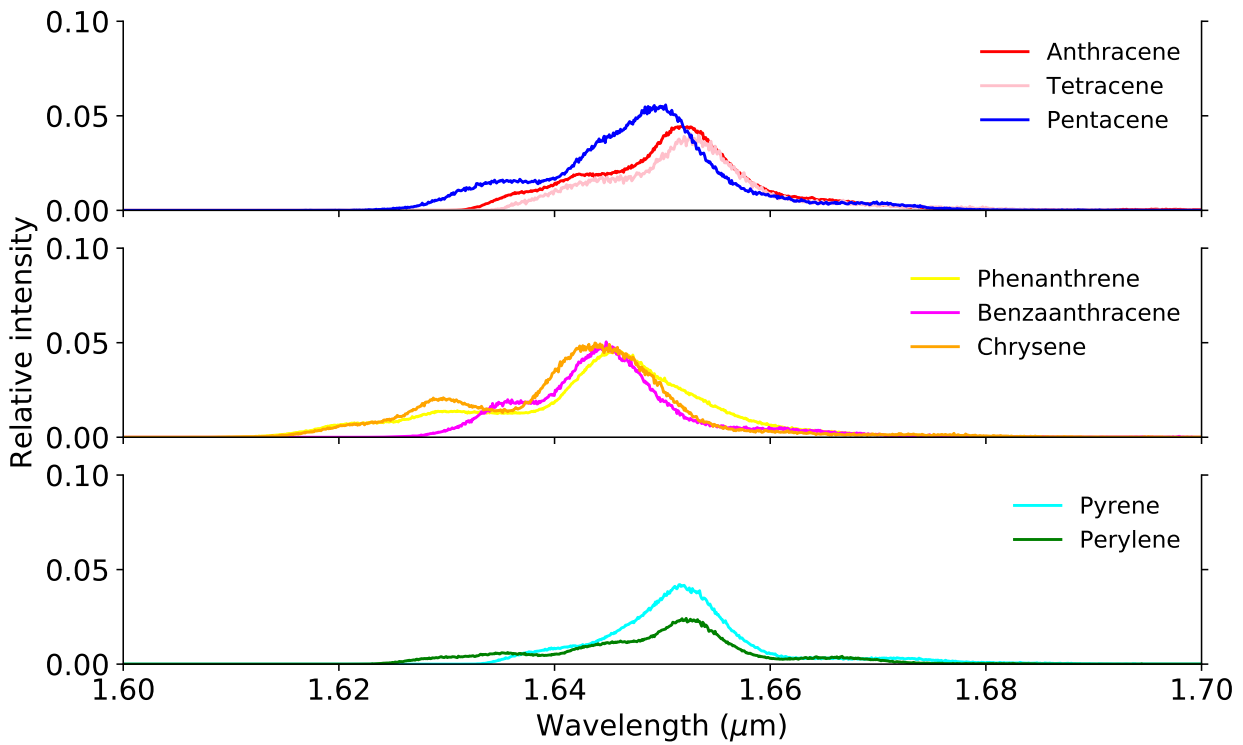


Fig. 6. The 1.6–1.7 μm region of the vibrationally-excited spectra of anthracene, tetracene, pentacene, phenanthrene, chrysene, benz[a]anthracene, pyrene and perylene at 1000 K.

Appendix

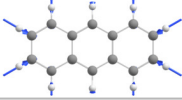
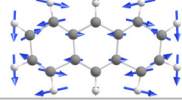
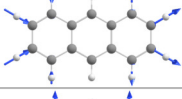
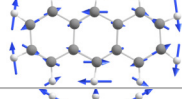
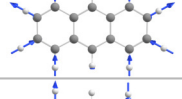
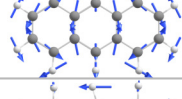
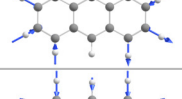
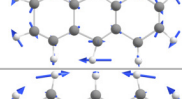
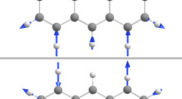
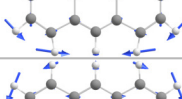
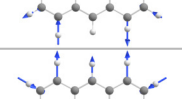
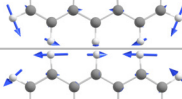
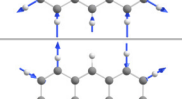
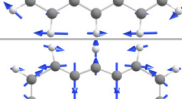
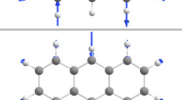
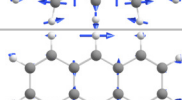
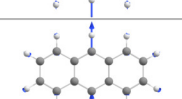
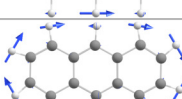
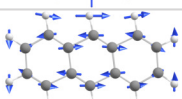
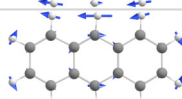


Mode	Frequency (cm ⁻¹)	Symmetry	Displacement vectors	Mode	Frequency (cm ⁻¹)	Symmetry	Displacement vectors
ν_1	3204.833	AG		ν_{12}	1672.287	B1U	
ν_2	3204.510	B2U		ν_{13}	1625.407	B3G	
ν_3	3193.047	B1U		ν_{14}	1599.218	AG	
ν_4	3192.859	B3G		ν_{15}	1583.753	B2U	
ν_5	3180.472	AG		ν_{16}	1518.713	AG	
ν_6	3179.393	B2U		ν_{17}	1486.548	B1U	
ν_7	3175.676	B1U		ν_{18}	1482.676	B2U	
ν_8	3175.200	B3G		ν_{19}	1437.236	AG	
ν_9	3171.641	AG		ν_{20}	1424.362	B2U	
ν_{10}	3169.791	B1U		ν_{21}	1411.787	B3G	
ν_{11}	1672.633	B3G		ν_{22}	1386.514	B2U	

Fig. 7. (Anthracene) Harmonic frequencies, symmetries and displacement vectors for the modes which contribute to the combination bands or overtones in the 1.6–1.7 μm and C–H stretching regions.

Appendix

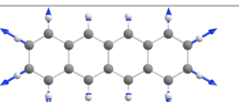
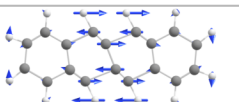
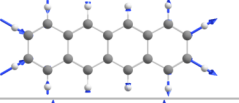
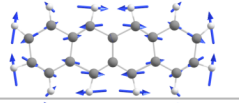
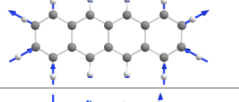
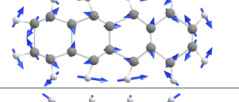
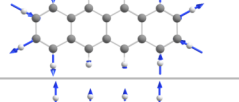
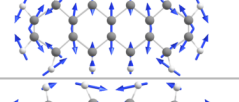
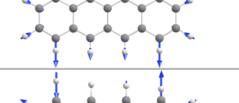
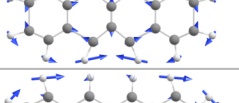
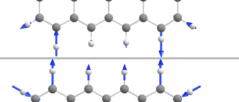
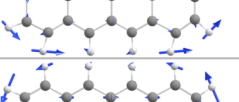
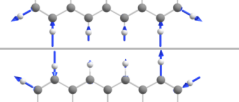
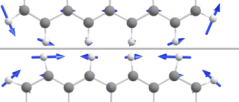
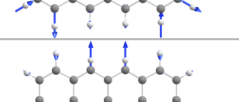
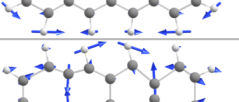
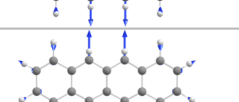
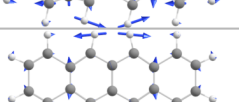
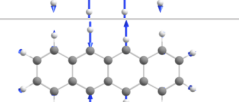
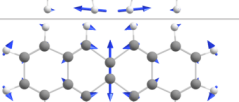
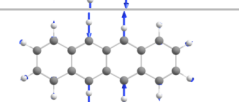
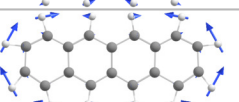
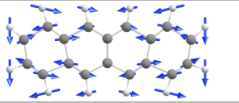
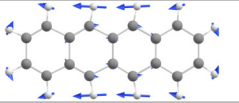
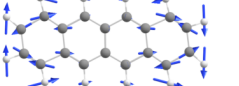

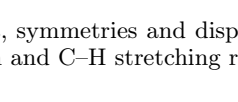
Mode	Frequency (cm ⁻¹)	Symmetry	Displacement vectors	Mode	Frequency (cm ⁻¹)	Symmetry	Displacement vectors
ν_1	3204.812	AG		ν_{15}	1653.386	B3G	
ν_2	3204.63	B2U		ν_{16}	1609.397	B1U	
ν_3	3193.151	B1U		ν_{17}	1588.122	B2U	
ν_4	3193.102	B3G		ν_{18}	1583.199	AG	
ν_5	3180.246	AG		ν_{19}	1561.266	AG	
ν_6	3179.671	B2U		ν_{20}	1503.278	B2U	
ν_7	3175.682	B1U		ν_{21}	1481.577	B3G	
ν_8	3175.437	B3G		ν_{22}	1480.869	AG	
ν_9	3174.377	AG		ν_{23}	1439.949	B2U	
ν_{10}	3172.157	B1U		ν_{24}	1432.132	AG	
ν_{11}	3170.958	B2U		ν_{25}	1421.679	AG	
ν_{12}	3169.366	B3G		ν_{26}	1415.935	B1U	
ν_{13}	1679.809	B1U		ν_{27}	1377.482	B2U	
ν_{14}	1664.762	B3G					

Fig. 8. (Tetracene) Harmonic frequencies, symmetries and displacement vectors for the modes which contribute to the combination bands or overtones in the 1.6–1.7 μm and C–H stretching regions.

Appendix

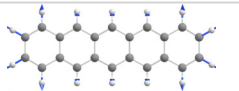
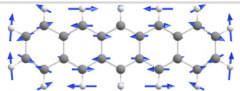
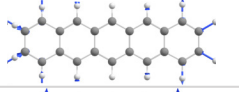
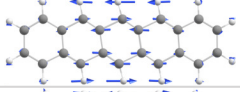
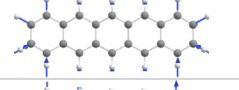
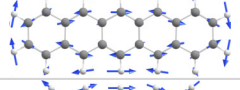
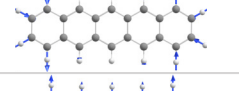
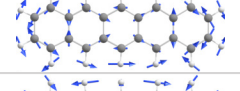
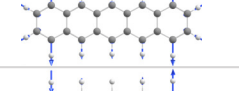
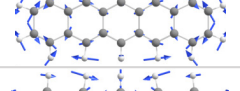
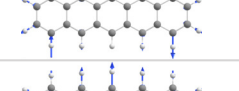
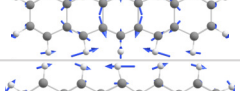
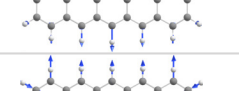
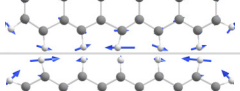
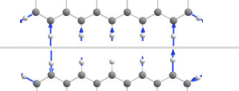
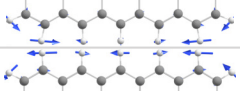
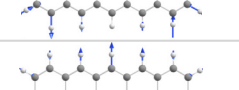
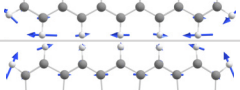
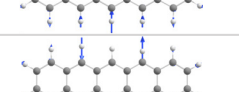
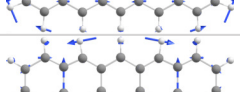
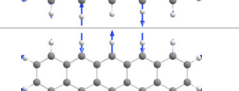
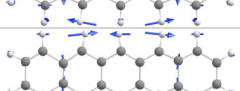
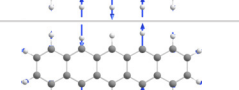
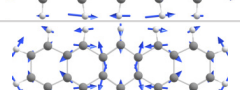
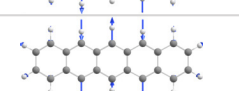
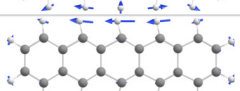
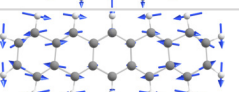
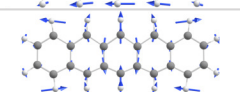
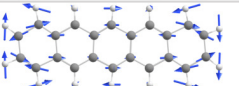
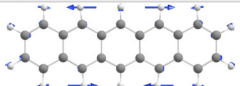
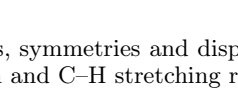
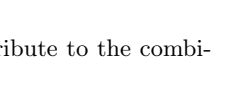
Mode	Frequency (cm ⁻¹)	Symmetry	Displacement vectors	Mode	Frequency (cm ⁻¹)	Symmetry	Displacement vectors
ν_1	3204.799	AG		ν_{17}	1643.779	B1U	
ν_2	3204.673	B2U		ν_{18}	1640.226	B3G	
ν_3	3193.209	B1U		ν_{19}	1594.744	B3G	
ν_4	3193.188	B3G		ν_{20}	1583.824	B2U	
ν_5	3180.116	AG		ν_{21}	1581.135	AG	
ν_6	3179.743	B2U		ν_{22}	1563.143	AG	
ν_7	3176.037	AG		ν_{23}	1546.121	B2U	
ν_8	3175.687	B1U		ν_{24}	1495.029	AG	
ν_9	3175.517	B3G		ν_{25}	1478.772	B2U	
ν_{10}	3173.614	B1U		ν_{26}	1478.262	B1U	
ν_{11}	3172.529	B2U		ν_{27}	1441.353	AG	
ν_{12}	3170.884	AG		ν_{28}	1434.148	B2U	
ν_{13}	3170.715	B3G		ν_{30}	1420.693	AG	
ν_{14}	3169.329	B1U		ν_{33}	1368.107	B2U	
ν_{15}	1676.842	B1U		ν_{35}	1317.907	B1U	
ν_{16}	1674.602	B3G		ν_{38}	1293.678	B1U	

Fig. 9. (Pentacene) Harmonic frequencies, symmetries and displacement vectors for the modes which contribute to the combination bands or overtones in the 1.6–1.7 μm and C–H stretching regions.

Appendix

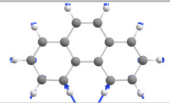
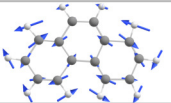
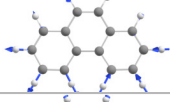
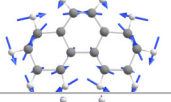
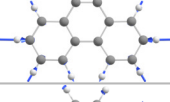
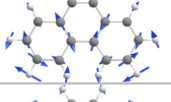
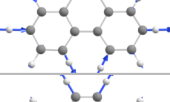
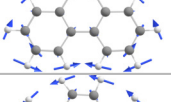
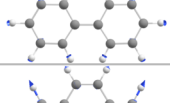
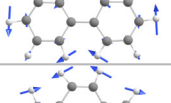
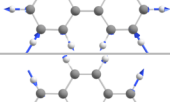
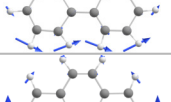
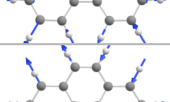
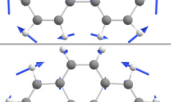
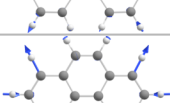
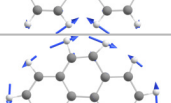
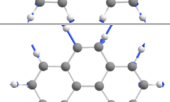
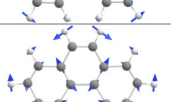
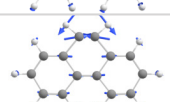
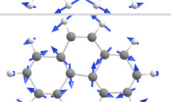


Mode	Frequency (cm ⁻¹)	Symmetry	Displacement vectors	Mode	Frequency (cm ⁻¹)	Symmetry	Displacement vectors
ν_1	3220.886	A1		ν_{12}	1658.864	B2	
ν_2	3209.107	B2		ν_{13}	1646.147	A1	
ν_3	3202.898	A1		ν_{14}	1612.380	B2	
ν_4	3199.865	B2		ν_{15}	1564.724	A1	
ν_5	3192.323	A1		ν_{16}	1537.450	B2	
ν_6	3187.909	A1		ν_{17}	1490.874	B2	
ν_7	3186.537	B2		ν_{18}	1471.571	A1	
ν_8	3177.006	B2		ν_{19}	1455.840	A1	
ν_9	3176.313	A1		ν_{20}	1445.036	B2	
ν_{10}	3173.451	B2		ν_{21}	1384.406	A1	
ν_{11}	1665.541	A1		ν_{22}	1381.224	B2	

Fig. 10. (Phenanthrene) Harmonic frequencies, symmetries and displacement vectors for the modes which contribute to the combination bands or overtones in the 1.6–1.7 μm and C–H stretching regions.

Appendix

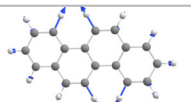
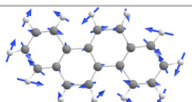
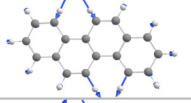
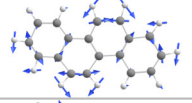
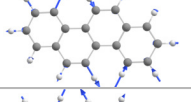
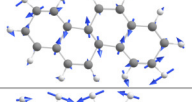
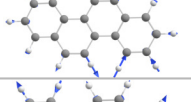
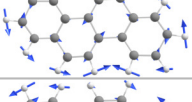
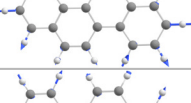
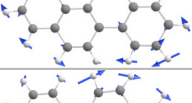
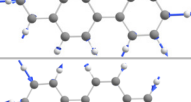
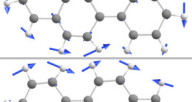
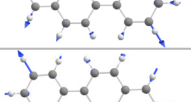
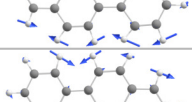
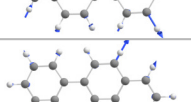
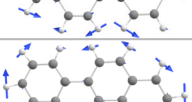
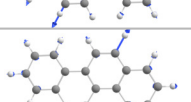
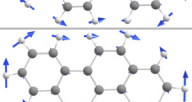
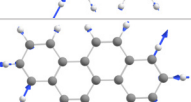
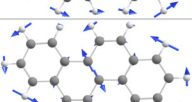
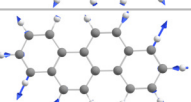
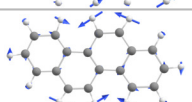
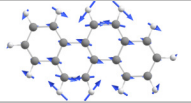
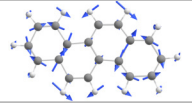
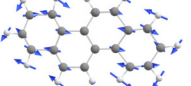
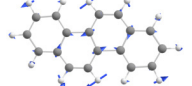
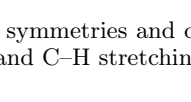
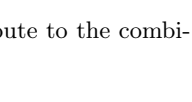
Mode	Frequency (cm ⁻¹)	Symmetry	Displacement vectors	Mode	Frequency (cm ⁻¹)	Symmetry	Displacement vectors
ν_1	3229.326	AG		ν_{15}	1650.493	AG	
ν_2	3229.065	BU		ν_{16}	1641.436	BU	
ν_3	3212.242	BU		ν_{17}	1611.073	AG	
ν_4	3212.079	AG		ν_{18}	1562.047	AG	
ν_5	3202.352	AG		ν_{19}	1559.187	BU	
ν_6	3202.084	BU		ν_{20}	1523.078	BU	
ν_7	3187.650	BU		ν_{21}	1485.354	AG	
ν_8	3187.308	AG		ν_{22}	1465.518	BU	
ν_9	3181.143	AG		ν_{23}	1463.363	AG	
ν_{10}	3180.386	BU		ν_{24}	1456.212	BU	
ν_{11}	3176.101	BU		ν_{25}	1403.337	AG	
ν_{12}	3175.941	AG		ν_{26}	1395.333	AG	
ν_{13}	1665.057	AG		ν_{27}	1394.526	BU	
ν_{14}	1661.569	BU		ν_{28}	1360.318	AG	

Fig. 11. (**Chrysene**) Harmonic frequencies, symmetries and displacement vectors for the modes which contribute to the combination bands or overtones in the 1.6–1.7 μm and C–H stretching regions.

Appendix

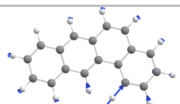
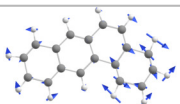
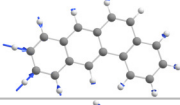
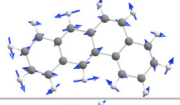
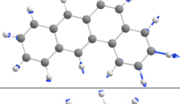
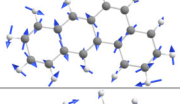
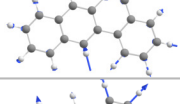
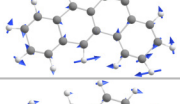
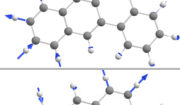
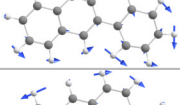
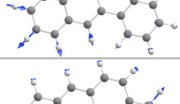
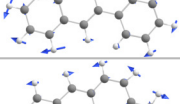
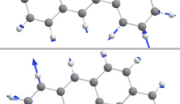
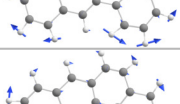
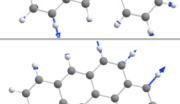
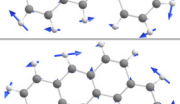
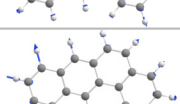
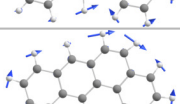
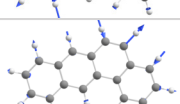
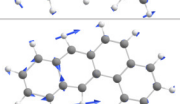
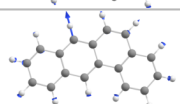
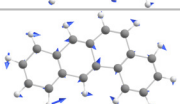
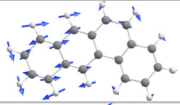
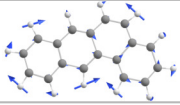
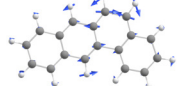

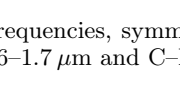
Mode	Frequency (cm ⁻¹)	Symmetry	Displacement vectors	Mode	Frequency (cm ⁻¹)	Symmetry	Displacement vectors
ν_1	3215.501	A'		ν_{15}	1652.712	A'	
ν_2	3204.450	A'		ν_{16}	1633.153	A'	
ν_3	3202.975	A'		ν_{17}	1603.529	A'	
ν_4	3194.500	A'		ν_{18}	1591.060	A'	
ν_5	3192.454	A'		ν_{19}	1537.582	A'	
ν_6	3192.095	A'		ν_{20}	1515.583	A'	
ν_7	3186.564	A'		ν_{21}	1487.562	A'	
ν_8	3178.884	A'		ν_{22}	1473.967	A'	
ν_9	3176.614	A'		ν_{23}	1457.295	A'	
ν_{10}	3174.595	A'		ν_{24}	1442.030	A'	
ν_{11}	3173.931	A'		ν_{25}	1426.468	A'	
ν_{12}	3170.047	A'		ν_{26}	1394.976	A'	
ν_{13}	1672.837	A'		ν_{27}	1376.203	A'	
ν_{14}	1666.526	A'					

Fig. 12. (Benz[a]anthracene) Harmonic frequencies, symmetries and displacement vectors for the modes which contribute to the combination bands or overtones in the 1.6–1.7 μm and C–H stretching regions.

Appendix

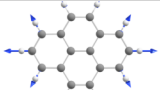
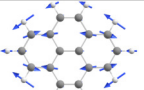
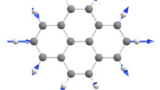
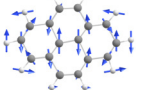
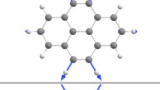
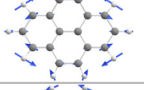
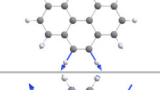
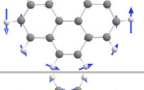
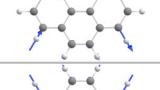
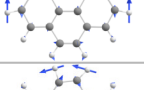
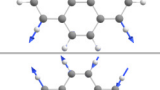
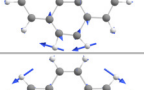
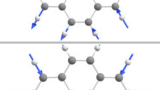
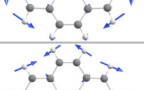
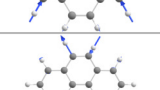
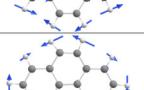
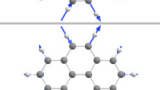
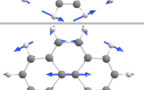
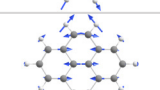
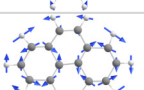
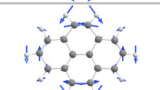
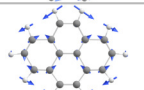


Mode	Frequency (cm ⁻¹)	Symmetry	Displacement vectors	Mode	Frequency (cm ⁻¹)	Symmetry	Displacement vectors
ν_1	3200.861	AG		ν_{13}	1638.223	B1U	
ν_2	3200.559	B1U		ν_{14}	1630.895	B3G	
ν_3	3191.798	AG		ν_{15}	1597.963	AG	
ν_4	3191.693	B2U		ν_{16}	1536.432	B3G	
ν_5	3183.995	B3G		ν_{17}	1520.005	B2U	
ν_6	3183.390	B2U		ν_{18}	1485.949	B1U	
ν_7	3176.839	B1U		ν_{19}	1460.161	B2U	
ν_8	3176.479	AG		ν_{20}	1460.073	B1U	
ν_9	3173.807	B3G		ν_{21}	1434.412	B3G	
ν_{10}	3173.527	B1U		ν_{22}	1433.771	AG	
ν_{11}	1675.414	AG		ν_{23}	1410.716	B3G	
ν_{12}	1648.961	B2U		ν_{24}	1354.954	B2U	

Fig. 13. (Pyrene) Harmonic frequencies, symmetries and displacement vectors for the modes which contribute to the combination bands or overtones in the 1.6–1.7 μm and C–H stretching regions.

Appendix

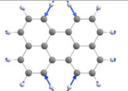
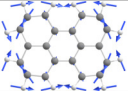
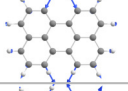
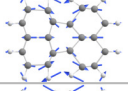
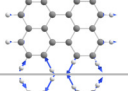
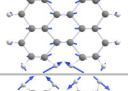
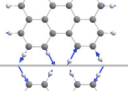
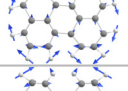
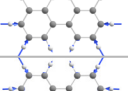
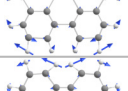
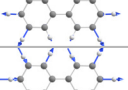
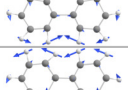
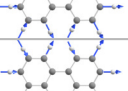
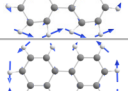
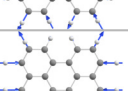
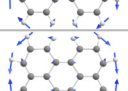
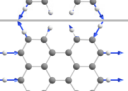
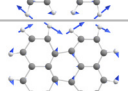
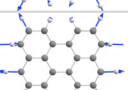
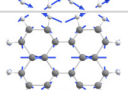
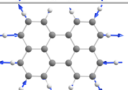
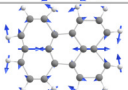
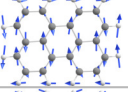
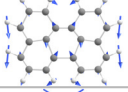
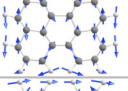
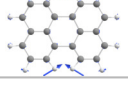
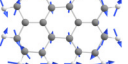

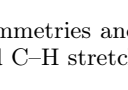
Mode	Frequency (cm ⁻¹)	Symmetry	Displacement vectors	Mode	Frequency (cm ⁻¹)	Symmetry	Displacement vectors
ν_1	3225.891	AG		ν_{16}	1634.004	AG	
ν_2	3225.748	B2U		ν_{17}	1629.851	B1U	
ν_3	3210.892	B1U		ν_{18}	1609.013	AG	
ν_4	3210.661	B3G		ν_{19}	1559.973	B3G	
ν_5	3198.566	AG		ν_{20}	1538.318	B2U	
ν_6	3197.157	B2U		ν_{21}	1508.725	B2U	
ν_7	3196.076	B1U		ν_{22}	1487.446	B3G	
ν_8	3194.844	B3G		ν_{23}	1474.354	B1U	
ν_9	3181.760	AG		ν_{24}	1472.309	AG	
ν_{10}	3181.190	B1U		ν_{25}	1409.844	B1U	
ν_{11}	3179.450	B2U		ν_{26}	1402.975	AG	
ν_{12}	3179.076	B3G		ν_{27}	1393.538	B1U	
ν_{13}	1664.168	B3G		ν_{30}	1362.452	B2U	
ν_{14}	1649.653	B2U		ν_{31}	1322.794	AG	
ν_{15}	1635.413	B1U					

Fig. 14. (Perylene) Harmonic frequencies, symmetries and displacement vectors for the modes which contribute to the combination bands or overtones in the 1.6–1.7 μm and C–H stretching regions.